RE.PUBLIC@POLIMI
Research Publications at Politecnico di Milano

Post-Print

This is the accepted version of:

P. Masarati
Robust Static Analysis Using General-Purpose Multibody Dynamics
Proceedings of the Institution of Mechanical Engineers Part K - Journal of Multi-body Dynamics, Vol. 229, N. 2, 2015, p. 152-165
doi:10.1177/1464419314554490

The final publication is available at https://doi.org/10.1177/1464419314554490

Access to the published version may require subscription.

When citing this work, cite the original published paper.

Permanent link to this version
http://hdl.handle.net/11311/854336

Robust Static Analysis Using General-Purpose Multibody Dynamics*

Pierangelo Masarati

Politecnico di Milano
Dipartimento di Scienze e Tecnologie Aerospaziali
via La Masa 34, 20156 Milano, Italy
tel: +39 02 2399 8309 fax: +39 02 2399 8334
email: *pierangelo.masarati@polimi.it*

October 3, 2014

Abstract

This works discusses the implementation of a pseudo-arc length algorithm in general-purpose multibody formulations. Such algorithm and implementation support the analysis of static problems subjected to bifurcations and turning points, expanding the applicability of such formulations. Its application to existing free general-purpose simulation software made the analysis of non-trivial static structural problems possible. Several examples of applications are presented and compared with existing solutions obtained from state-of-the-art formulations.

Keywords: Static Analysis, Continuation, Bifurcation, Arc-Length, Multibody Dynamics

1 Introduction

Computational methods that are characteristic of nonlinear dynamics have been applied for over 35 years to the static analysis of structures to address problems associated with incremental loading past critical points.

In 1977, Haisler et al. proposed a displacement incrementation in non-linear structural analysis using what they termed the self-correcting method [1]. In 1979, Batoz and Dhatt developed incremental displacement algorithms for nonlinear problems [2]. In 1979, in a seminal work Riks proposed an incremental approach to the solution of snapping and buckling problems [3]. Shortly after, in 1981, Crisfield proposed a fast incremental/iterative solution procedure capable of handling "snap-through" [4] and, in 1983, an arc-length method that takes into account line searches and accelerations [5]. In 1984, Meek and Tan developed a geometrically nonlinear analysis of space frames using an incremental iterative technique [6]. In 1986, Schweizerhof and Wriggers presented a consistent linearization for path following methods in nonlinear FE analysis [7]. In 1987, Forde and Stiemer proposed improved arc length orthogonality methods suitable for nonlinear finite element analysis [8]. In 1989, Meek and Loganathan studied the geometrically non-linear behaviour of space frame structures [9]. At the same time, Kouhia and Mikkola worked at tracing equilibrium paths beyond simple critical points [10]. In 1990, Clarke and Hancock studied incremental-iterative strategies for non-linear analysis [11]. In 1991, Chen and Schreyer proposed structural solution strategies based on the secant approach considering

*The final, definitive version of this paper has been published in *Part K: Journal of Multi-body Dynamics*, Vol/Issue, Month/Year `http://dx.doi.org/10.1177/1464419314554490` by SAGE Publications Ltd, All rights reserved.
© [IMechE]

element constraints for incremental damage [12]. In 1993, Allgower and Georg investigated continuation and path following for structural analysis [13]. In 1994, Carrera discussed operation failures of methods based on arc-length approximations [14]. In 1995, Feng et al. addressed the problem of determining travel directions in path-following methods [15], and shortly after proposed a new criterion for determining the initial loading parameter in arc-length methods [16]. In 1996, Lazopoulos analyzed second order displacement fields of thick elastic plates under thrust [17]; with Markatis, Lazopoulos also studied compound branching in elastic systems [18]. At the same time, Cardona and Huespe discussed path following with turning and bifurcation points in the analysis of multibody systems [19], with specific reference to problems involving finite rotations [20]. In 1998, Hellweg and Crisfield proposed a new arc-length method for handling sharp snap-backs [21]. In 1999, de Souza Neto and Feng discussed the determination of the path direction for arc-length methods in the presence of bifurcations and snapbacks [22]. In 2000, Taheri and Moradi developed a robust methodology for the simulation of the postbuckling response of composite plates [23]. In 2001, Choong and Kim proposed a numerical strategy based on a generalized inverse and the continuation method to compute the stability boundaries for multi-loading systems [24]. At the same time, Georg proposed a matrix-free approach for numerical continuation and bifurcation, [25]. In 2002, Eriksson and Pacoste proposed numerical techniques for stability problems in shells, along with an element formulation [26]. In 2004, Riks presented a detailed review of numerical methods for the study of buckling in chapter 4 of [27]. At the same time, Mallardo and Alessandri discussed the implementation of arc-length procedures with BEM in nonlinear problems [28], and Memon and Su developed a specific arc-length technique for nonlinear finite element analysis [29], whereas Yuanqi and Zuyan proposed improvements to the arc-length-type method [30]. In 2007, Müller compared the use of a stabilized Newton-Raphson scheme to the arc-length method applied to the overcoming of instability points in FEM problems [31]. In 2008, Ritto-Corrêa and Camotim reviewed the arc-length and other quadratic control methods in view of several implementation procedures [32]. At the same time, Houhia worked at stabilized forms of orthogonal residual and constant incremental work control path following methods [33].

The available literature testifies at the same time the maturity and the interest in the development of robust, reliable and effective techniques for the analysis of nonlinear structural problems when static stability is a concern. The proposed literature review also indicates that such interest is confined, so to speak, in the nonlinear finite element community, whereas the multibody dynamics community seems to lack such interest. In many cases, buckling is seen as a degeneration of a dynamic problem, and post-bucking is analyzed by increasing loads at a very slow rate, often as a 'slow' dynamic buckling problem to rely on inertia as a means to capture snapthrough. At the same time, flexible multibody dynamics has developed towards nonlinear finite elements by introducing very sophisticated beam, (e.g. the so-called Geometrically Exact Beam Formulation, GEBF), shell, and membrane models.

This work is not proposing a new method. Its aim is to illustrate how existing arc-length-type methods can be easily and effectively applied to existing multibody dynamics formulations that were initially formulated for the solution of dynamic problems, i.e. the vast majority of multibody formulations currently in development and use in the academia and in the industry. For this purpose, no specific details are given on the formulation of the structural mechanics within the multibody solver. On the contrary, the generality of the approach leverages whatever deformable components (lumped components, beams, shells, and so on) are provided by the underlying solver. In the author's knowledge, this possibility has not been addressed yet in the field of multibody dynamics, with the notable partial exception of the previously mentioned early works of Cardona and Huespe [19, 20].

The solution of static problems usually requires parametrized problems of the form

$$\mathbf{r}\left(\mathbf{x}, p\right) = \mathbf{0} \tag{1}$$

to be solved with respect to $\mathbf{x}$ for a given set of values of the parameter p. In Eq. (1), vector $\mathbf{x} \in \mathbb{R}^n$ collects the degrees of freedom of the problem (e.g. nodal displacements and rotations in a FEM-like

model); $p \in \mathbb{R}$ is a scalar load increment parameter, and $\mathbf{r} : \mathbb{R}^{n+1} \mapsto \mathbb{R}^n$ is the residual that needs to vanish at convergence.

A solution $\overline{\mathbf{x}}$ is sought for $p = \overline{p}$; when the problem of Eq. (1) is non-linear, multiple solutions (or none) can exist, and the "right" (namely, the desired) solution may be path-dependent. Moreover, solving the problem of Eq. (1) using a Newton-like iteration requires the process to start from within a "good" neighbor of the solution, whose guess may not be easy.

A common approach consists in incrementing p from a suitable initial value (e.g. 0, corresponding to an unloaded system) to the desired value (or as much as possible, when an ultimate value is sought), in a so-called *continuation* process. However, the problem may easily become ill-posed as soon as the solution needs to overcome snapthrough conditions or other types of limit points. In these cases, the problem becomes (nearly) singular, and even very small load increments imply very large changes in configuration as the Jacobian matrix[1] $\mathbf{r}_{/\mathbf{x}}$ becomes (nearly) singular. At critical points, $\mathbf{r}_{/\mathbf{x}}$ is singular[2]. If $\mathbf{r}_{/p}$ belongs to the range of $\mathbf{r}_{/\mathbf{x}}$, the critical point is a limit point; otherwise, it is a bifurcation. In some cases, the load may actually need to *reduce*, e.g. past a limit point, or the point of application of the load may even need to temporarily revert the sign of its displacement increment to let the solution evolve along a path different from the one followed during loading so far, e.g. past bifurcation and turning points.

Load evolution strategies that prescribe the growth of the load or of some component of the displacement of specific points may lead to singular points of this kind. *Global* measures of the evolution of the solution are better suited to turn a locally singular into a globally regular process.

2 Approach

Following the approach proposed by Riks in 1979 [3], the problem of Eq. (1) is extended by introducing a load increment procedure that corresponds to controlling a measure of the arc length of the solution in a new space $\mathbf{y}$ that expands the original solution space $\mathbf{x}$ by including the original load increment parameter p, namely $\mathbf{y} = \{\mathbf{x}; p\} \in \mathbb{R}^{n+1}$.

Let us assume that the solution can be parametrized with a scalar parameter $\eta \in \mathbb{R}$ such that $\mathbf{x} = \mathbf{x}(\eta)$ and $p = p(\eta)$; the infinitesimal arc length is

$$\mathrm{d}s = \left(\mathbf{y}_{/\eta}^T \mathbf{y}_{/\eta}\right)^{1/2} \mathrm{d}\eta. \tag{2}$$

An appropriate metric of the new space may be useful to improve the numerical treatment of the solution and to 'guide' the selection of the load increment; the weighted infinitesimal arc length definition is

$$\mathrm{d}s = \left(\mathbf{y}_{/\eta}^T \mathbf{W} \mathbf{y}_{/\eta}\right)^{1/2} \mathrm{d}\eta, \tag{3}$$

where $\mathbf{W}$ is a suitably chosen weight matrix (e.g. such that dimension homogeneity is restored among displacement, rotation and load variables).

When a load increment needs to be considered, in order to transition from solution $\overline{\mathbf{y}}$ to $\mathbf{y} = \overline{\mathbf{y}} + \Delta\mathbf{y}$, with $\Delta\mathbf{y}$ corresponding to the solution increment caused by a finite although arbitrary load increment, the corresponding discrete arc length can be approximated as $\Delta s \cong (\Delta\mathbf{y}^T \mathbf{W} \Delta\mathbf{y})^{1/2}$.

Consider now the solution of the problem at a specific increment value; the original problem becomes

$$\mathbf{0} = -\mathbf{r}\left(\overline{\mathbf{y}} + \Delta\mathbf{y}\right) \tag{4a}$$

$$0 = \Delta s - \left(\Delta\mathbf{y}^T \mathbf{W} \Delta\mathbf{y}\right)^{1/2}. \tag{4b}$$

[1] The symbol $(\spadesuit)_{/(\clubsuit)}$ indicates the partial derivative of $(\spadesuit)$ with respect to $(\clubsuit)$.

[2] In this work we only consider the case of order one nullspace of $\mathbf{r}_{/\mathbf{x}}$.

Its solution using the Newton-Raphson algorithm requires the iterative solution of the problem

$$\mathbf{r}_{/\mathbf{y}}\delta\mathbf{y} = -\mathbf{r}\left(\overline{\mathbf{y}} + \Delta\mathbf{y}\right) \tag{5a}$$

$$\frac{\Delta\mathbf{y}^T\mathbf{W}}{\left(\Delta\mathbf{y}^T\mathbf{W}\Delta\mathbf{y}\right)^{1/2}}\delta\mathbf{y} = \Delta s - \left(\Delta\mathbf{y}^T\mathbf{W}\Delta\mathbf{y}\right)^{1/2}, \tag{5b}$$

with $\Delta\mathbf{y}$ += $\delta\mathbf{y}$ until convergence; Δs is suitably chosen to represent the desired increment in the arc length of the solution in the new space; this includes the actual load increment itself, Δp.

The strategy corresponding to prescribing the increment of either the load or a configuration component is obtained by setting to zero the entire matrix $\mathbf{W}$, except for the diagonal entry corresponding to the load p or to that specific configuration component.

The approach under discussion fails when $\overline{\mathbf{y}} = \{\overline{\mathbf{x}}; \overline{p}\}$ corresponds to a bifurcation point, i.e. a point in $\mathbf{y}$ for which $\mathbf{r}_{/p}$ belongs to the range of $\mathbf{r}_{/\mathbf{x}}$. In such case, the augmented problem of Eqs. (5) is still structurally singular. Two more equations need to be added: one that expresses the null vector[3], of $\mathbf{r}_{/\mathbf{x}}$, $\mathbf{v}$,

$$\mathbf{r}_{/\mathbf{x}}\mathbf{v} = -\mathbf{v}\lambda = \mathbf{0} \tag{6}$$

(since λ, the eigenvalue, is zero), and one for the normalization of such eigenvector:

$$\mathbf{v}^T\mathbf{v} = 1. \tag{7}$$

A contribution $\mathbf{v}\lambda$ can be added also to Eq. (4a), since it is zero (in fact, since $\mathbf{r}(\overline{\mathbf{y}}) \equiv \mathbf{0}$ at bifurcation, λ is null). however, thanks to such contribution, the matrix of the linearized problem

$$\begin{bmatrix} \mathbf{r}_{/\mathbf{y}} & \mathbf{0} & \mathbf{v} \\ (\Delta\mathbf{y}^T\mathbf{W}\Delta\mathbf{y})^{-1/2}\Delta\mathbf{y}^T\mathbf{W} & \mathbf{0}^T & 0 \\ \mathbf{0} & \mathbf{r}_{/\mathbf{x}} & \mathbf{v} \\ \mathbf{0}^T & \mathbf{v}^T & 0 \end{bmatrix} \begin{Bmatrix} \delta\mathbf{y} \\ \delta\mathbf{v} \\ \delta\lambda \end{Bmatrix} = \begin{Bmatrix} -\mathbf{r} - \mathbf{v}\lambda \\ \Delta s - (\Delta\mathbf{y}^T\mathbf{W}\Delta\mathbf{y})^{1/2} \\ -\mathbf{r}_{/\mathbf{x}}\mathbf{v} - \mathbf{v}\lambda \\ (1 - \mathbf{v}^T\mathbf{v})/2 \end{Bmatrix} \tag{8}$$

is no longer singular. In fact, the first block row of the matrix in Eq. (8) contains $\mathbf{r}_{/\mathbf{x}}$ and $\mathbf{v}$, which by construction is the null vector of $\mathbf{r}_{/x}$.

This aspect is not deemed critical, since the determination of bifurcation points is not the aim of the present work; as such, this capability has not been pursued further. In practical path following, bifurcations are avoided by introducing small load perturbations that cause the solution to progress along stable paths, as illustrated in some of the subsequent examples.

2.1 Prediction

The prediction of the new increment plays a fundamental role in the solution strategy to solve nonlinear problems in the vicinity of buckling or snapthrough, where the load may actually need to reduce in order to progress with the solution.

A continuation procedure may be used to ensure that the prediction 'suggests' the solution to progress along the appropriate direction in the space $\mathbf{y}$. This can be obtained by considering the derivative of the problem with respect to η,

$$\mathbf{0} = -\mathbf{r}_{/\mathbf{y}}\mathbf{y}_{/\eta} \tag{9a}$$

$$0 = s_{/\eta} - \left(\mathbf{y}_{/\eta}^T\mathbf{W}\mathbf{y}_{/\eta}\right)^{1/2}. \tag{9b}$$

[3]The eigenvector that corresponds to the null eigenvalue, which is assumed to have unit algebraic multiplicity.

Its linearization yields

$$\mathbf{r}_{/\mathbf{y}}\delta\mathbf{y}_{/\eta} = -\mathbf{r}_{/\mathbf{y}}\mathbf{y}_{/\eta} \tag{10a}$$

$$\left(\mathbf{y}_{/\eta}^T\mathbf{W}\mathbf{y}_{/\eta}\right)^{-1/2}\mathbf{y}_{/\eta}^T\mathbf{W}\delta\mathbf{y}_{/\eta} = s_{/\eta} - \left(\mathbf{y}_{/\eta}^T\mathbf{W}\mathbf{y}_{/\eta}\right)^{1/2} \tag{10b}$$

with $s_{/\eta}$ arbitrary (e.g. equal to 1). The resulting $\mathbf{y}_{/\eta}$ can be used to predict an accurate estimate of the new tentative value of $\mathbf{y}$ for a given increment $\Delta\eta$.

The problem is formally analogous to that of Eqs. (5), with $\Delta\mathbf{y}$ replaced by $\mathbf{y}_{/\eta}$; however, its convergence should be extremely fast, since it is now essentially linear, the only nonlinear part being confined in the normalization of the solution. In fact, the residual $\mathbf{r}(\mathbf{y})$ no longer appears in the formula; on the contrary, only the Jacobian matrix $\mathbf{r}_{/\mathbf{y}}$ evaluated for a fixed $\mathbf{y}$ is needed, which is already available.

More sophisticated prediction strategies may be designed and exploited; in practice, at least in the cases presented in Section 4, no specific strategy was required. Indeed, the prediction of the numerical scheme implemented in the general-purpose multibody solver and originally intended for the solution of smooth initial value problems [34] has been successfully used. The prediction of the derivative of the state is a third-order extrapolation from the state and its derivative at two previous steps using cubic Hermitian functions, whereas the prediction of the state is a second-order extrapolation based on an implicit, A/L stable two-step integration scheme. For the sake of completeness, the method is briefly summarized in the following; further details have been recently presented in [34].

In practice, given $\mathbf{y}_{k-1}$, $\dot{\mathbf{y}}_{k-1}$, and $\mathbf{y}_{k-2}$, $\dot{\mathbf{y}}_{k-2}$ at the two time steps before the yet unknown step k, where what is formally a time derivative practically becomes a derivative with respect to the loading parameter[4], i.e. $\dot{\mathbf{y}} \to \mathbf{y}_{/s} = \mathring{\mathbf{y}}$, the prediction for step k gives

$$\mathring{\mathbf{y}}_k = \frac{1}{\Delta s}\left(m_1\mathbf{y}_{k-1} + m_2\mathbf{y}_{k-2}\right) + n_1\mathring{\mathbf{y}}_{k-1} + n_2\mathring{\mathbf{y}}_{k-2} \tag{11}$$

$$\begin{aligned}\mathbf{y}_k &= a_1\mathbf{y}_{k-1} + a_2\mathbf{y}_{k-2} + \Delta s\left(b_0\mathring{\mathbf{y}}_k + b_1\mathring{\mathbf{y}}_{k-1} + b_2\mathring{\mathbf{y}}_{k-2}\right)\\ &= \left(a_1 + b_0m_1\right)\mathbf{y}_{k-1} + \left(a_2 + b_0m_2\right)\mathbf{y}_{k-2} + \Delta s\left(\left(b_1 + b_0n_1\right)\mathring{\mathbf{y}}_{k-1} + \left(b_2 + b_0n_2\right)\mathring{\mathbf{y}}_{k-2}\right),\end{aligned} \tag{12}$$

with

$$\begin{aligned} m_1 &= -12 & n_1 &= 8\\ m_2 &= 12 & n_2 &= 5\\ & & b_0 &= \delta + 1/2\\ a_1 &= 1 - \beta & b_1 &= \beta/2 + 1/2 - 2\delta\\ a_2 &= \beta & b_2 &= \beta/2 + \delta\\ \beta &= \frac{3\left(1 - |\rho_\infty|\right)^2 + 4\left(2\,|\rho_\infty - 1|\right)}{4 - \left(1 - |\rho_\infty|\right)^2} & \delta &= \frac{\left(1 - |\rho_\infty|\right)^2}{2\left(4 - \left(1 - |\rho_\infty|\right)^2\right)}; \end{aligned}$$

$|\rho_\infty|$ is the asymptotic spectral radius of the method, a parameter that can be tuned between 1 and 0 to control the algorithmic dissipation ($|\rho_\infty| = 0$ yields the L-stable second-order Backward Difference Formulas; an optimal value is $|\rho_\infty| \approx 0.6$, as discussed in [34]).

It is worth noticing that the algebraic variables, e.g. those that express the Lagrange multipliers, are internally treated (e.g. predicted) as state derivatives. Nodal displacements and rotations are treated as states; their state derivatives lose meaning in a static analysis, but are internally considered in the solution process, specifically during the prediction.

[4]Derivation with respect to the loading parameter from this point on is indicated as $(\clubsuit)_{/s} = \mathring{(\clubsuit)}$.

It is also worth stressing that the details about the integration method are simply given to provide complete information about the procedure used to compute the results that are presented in Section 4; the notion of spectral radius of the numerical integration scheme is meaningless in the context of a static analysis.

3 Implementation

The implementation of the pseudo-arc length load increment control in existing analysis is straightforward. Two user-defined elements need to be created: a 'load increment normalization' element, complemented by one or more 'load increment force' elements. They are described in the following.

3.1 Load Increment Force and Moment

Consider Eqs. (5): the Jacobian matrix of Eq. (5a), $\mathbf{r}_{/\mathbf{y}}$, is the original Jacobian matrix of a usual static problem (i.e. with static nodes only), $\mathbf{r}_{/\mathbf{x}}$, augmented by the last column that contains the partial derivative of the residual with respect to the original load increment, $\mathbf{r}_{/p}$. This latter contribution is new and must be specifically implemented. It is delegated to a specially designed 'load increment force' element that assembles its contribution to $\mathbf{r}$, $\mathbf{r}_{/\mathbf{x}}$, if any, and $\mathbf{r}_{/p}$. The contributions to $\mathbf{r}$, $\mathbf{r}_{/\mathbf{x}}$ are identical to those of regular external force (moment) elements where a force (moment) along (about) a fixed direction, either in the global or in a local reference frame, is multiplied by a scalar p.

Force. A force acting on node i along direction $\mathbf{e}$ gives the force and moment

$$\mathbf{f}_i = \mathbf{e}p \tag{13a}$$

$$\mathbf{m}_i = \mathbf{o}_i \times \mathbf{f}_i, \tag{13b}$$

where $\mathbf{o}_i = \mathbf{R}_i\tilde{\mathbf{o}}_i$ is the offset of the force application point with respect to the node.

When the direction of the force is fixed in the global reference frame the unit vector $\mathbf{e}$ is constant. As a consequence, the linearization of force and moment contributions of Eqs. (13) yields

$$\delta\mathbf{f}_i = \mathbf{e}\delta p \tag{14a}$$

$$\begin{aligned}\delta\mathbf{m}_i &= \mathbf{o}_i \times \delta\mathbf{f}_i + \delta\mathbf{o}_i \times \mathbf{f}_i \\ &= \mathbf{o}_i \times \mathbf{e}\delta p + \mathbf{f}_i \times \mathbf{o}_i \times \boldsymbol{\theta}_{i\delta},\end{aligned} \tag{14b}$$

where $\boldsymbol{\theta}_{i\delta}$ is the virtual rotation of node i, such that $\delta\mathbf{R} = \boldsymbol{\theta}_\delta \times \mathbf{R}$ and thus $\delta\mathbf{o}_i = \boldsymbol{\theta}_{i\delta} \times \mathbf{o}_i$.

When the direction of the force is fixed in the reference frame of the node, in the global reference frame it is expressed as $\mathbf{e} = \mathbf{R}_i\tilde{\mathbf{e}}$, where the unit vector $\tilde{\mathbf{e}}$ is the (constant) direction in the node reference frame. The linearization of the force yields

$$\delta\mathbf{f}_i = \mathbf{e}\delta p - \mathbf{f}_i \times \boldsymbol{\theta}_{i\delta} \tag{15a}$$

$$\delta\mathbf{m}_i = \mathbf{o}_i \times \mathbf{e}\delta p - \mathbf{m}_i \times \boldsymbol{\theta}_{i\delta}. \tag{15b}$$

Moment. A moment acting on node i about direction $\mathbf{e}$ gives the moment

$$\mathbf{m}_i = \mathbf{e}p \tag{16}$$

When the direction of the moment is fixed in the global reference frame, vector $\mathbf{e}$ is constant. As a consequence, the linearization of the moment yields

$$\delta\mathbf{m}_i = \mathbf{e}\delta p. \tag{17}$$

When the direction of the moment is fixed in the reference frame of the node, it is expressed as $\mathbf{e} = \mathbf{R}_i\tilde{\mathbf{e}}$. The linearization of the moment yields

$$\delta\mathbf{m}_i = \mathbf{e}\delta p - \mathbf{m}_i \times \boldsymbol{\theta}_{i\delta}. \tag{18}$$

3.2 Load Increment Normalization

The Jacobian matrix of Eq. (5b) is easily assembled from the increment in the state variables, $\Delta\mathbf{x}$, plus that of a newly defined 'private' algebraic variable p of a specifically implemented 'load increment normalization' element, which is essentially analogous to an arbitrary kinematic constraint $\phi(\mathbf{x}, \lambda) = 0$, enforced using a Lagrange multiplier λ,

$$\mathbf{r}(\mathbf{x}) + \phi'^{T}_{\mathbf{x}}\lambda = \mathbf{0} \tag{19a}$$

$$\phi(\mathbf{x}) = 0. \tag{19b}$$

This element takes care of instantiating Eq. (5b), in partial analogy with Eq. (19b), and the variable corresponding to p. The analogy with Eqs. (19) ends here: the analogous of the contribution $\phi'^{T}_{\mathbf{x}}\lambda$ in Eq. (19a) is actually one or more instances of the previously mentioned load increment force element, where the load variable p plays the role of the Lagrange multiplier λ. A formal analogy may be found with the control constraint problem (see for example [35]), with the load increment normalization equation, Eq. (4b), playing the role of the trajectory specification equation, and the load increment force element playing the role of the control constraint forces.

The load increment normalization element must be able to access the model data manager to extract information about $\mathbf{x}$ and $\Delta\mathbf{x}$. Since the estimate of the finite arc length increment needs not be accurate, as long as it succeeds in making the problem non singular, one may legitimately decide to only consider position increments, thus eliminating the burden associated with handling of finite rotations. This corresponds to selectively setting to zero the coefficients of matrix $\mathbf{W}$ associated with rotation parameters.

4 Numerical Examples

This section illustrates the implementation of the approximate arc-length approach in MBDyn by means of several examples, most of which have been taken from the open literature.

4.1 Nonlinear Bi-stable Spring

Consider the problem $r(x, p) = k_1 x + k_3 x^3 - p$ with $k_1 = -1$, $k_3 = 1$, starting from the (stable) initial solution $x = -\sqrt{-k_1/k_3} = -1$, $p = 0$ and a load increment strategy where the finite arc length is normalized with $\mathbf{W} = \mathbf{I}_{2\times 2}$. When increments $\Delta s = 0.2$ are considered while $p \leq 4$, the curve of Fig. 1 is obtained, which involves a substantial reduction of p to pass through the (unstable) solution $x = 0$ and then through the stable solution $x = \sqrt{-k_1/k_3} = 1$, both for $p = 0$.

4.2 Snap-Through Buckling of a Hinged Right-Angle Frame

This 2D problem, discussed by many authors, has been recently presented in [32]. As shown in Fig. 2, the structure is a right-angle frame made of two identical beams that form a right angle at one common end and are connected to the ground at the other ends by revolute hinges that allow rotation about two axes orthogonal to the plane formed by the frame.

A force along an absolute direction that is initially orthogonal to one of the beams is applied at one fifth of the beam length from the frame angle. In accordance with [36], relevant data are collected in Table 1. In the present work this problem is analyzed using the original finite volume beam formulation implemented in MBDyn, which was first presented in [37]. In accordance with Refs. [36, 32], the model is discretized using five three-node beam elements for each beam of the frame. As discussed in [37], the mentioned finite volume approach for C^0 beam elements does not require selective relaxation of the integration to avoid shear locking.

Figure 3(a) shows the vertical and horizontal components, in the global reference frame, of the displacement of the point where the load is applied and the corresponding load value. The results are

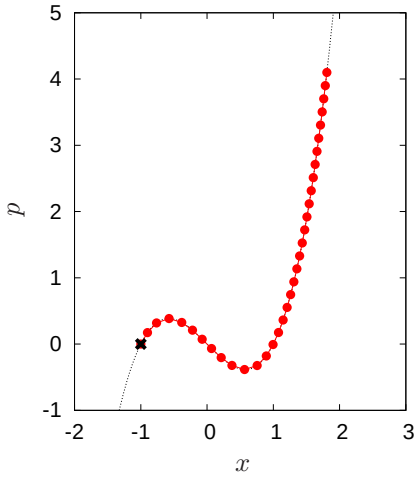

Figure 1: Nonlinear bi-stable spring.

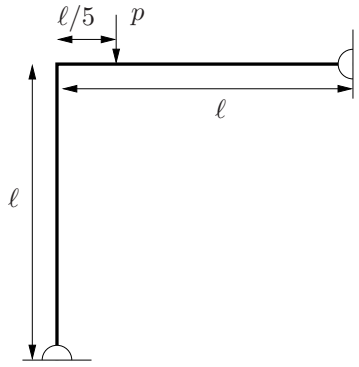

Figure 2: Hinged right-angle frame sketch.

Table 1: Hinged right-angle frame non-dimensional data.

Length, ℓ	120.0
Inertia	2.0
Area	6.0
Young's modulus	7.2×10^6
Poisson's ratio	0.3

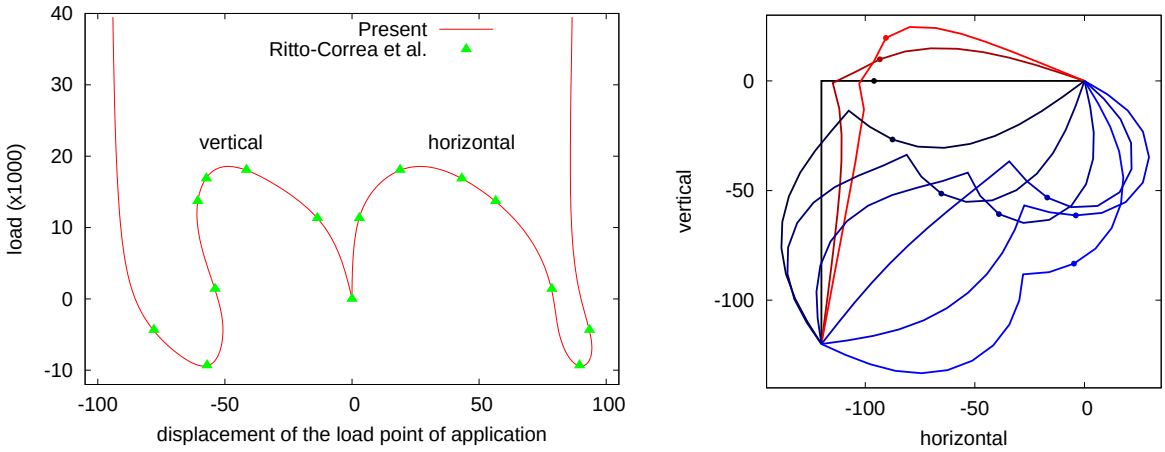

(a) Load vs. displacement components of load application point.

(b) Deformed shapes.

Figure 3: Snap-through buckling of a hinged right-angle frame

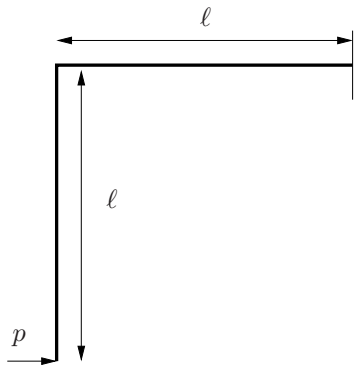

Figure 4: Right-angle frame sketch.

coincident with those reported in [32]. Figure 3(b) shows some deformed shapes for both positive (upward pull) and negative (downward push) initial loading; the circle indicates the point of application of the force, directed along the vertical.

4.3 Lateral-Torsional Buckling of Right-Angle Frame

This 3D problem, discussed by many authors, has been recently presented in [32]. As shown in Fig. 4, the structure is a right-angle frame made of two identical beams that form a right angle at one common end. The horizontal beam is clamped at the other end.

A horizontal force is applied at the free end of the vertical beam. The force does not exactly lie in the plane formed by the two beams; a component orthogonal to such plane and equal to 1/1000 of the in-plane component causes the response to follow the stable bifurcated path. The load is applied in such a manner that the horizontal bar is alternatively loaded in tension and in compression. In accordance with [36], relevant data are collected in Table 2. The shear factor κ multiplied by GA yields the shear stiffness. The problem is analyzed using a two-node variant of the previously mentioned finite volume beam formulation, also implemented in MBDyn, which was recently presented in [38]. 10 two-node beam elements are used for each beam.

Figure 5 presents the in-plane load as a function of the horizontal displacement of the free end of

Table 2: Right-angle frame non-dimensional data.

Length, ℓ	240.0
Section width, b	0.6
Section height, h	30.0
Young's modulus	7.124×10^4
Poisson's ratio	0.31
Shear factor, κ	5/6
Torsional constant, J_p	$bh^3/3$

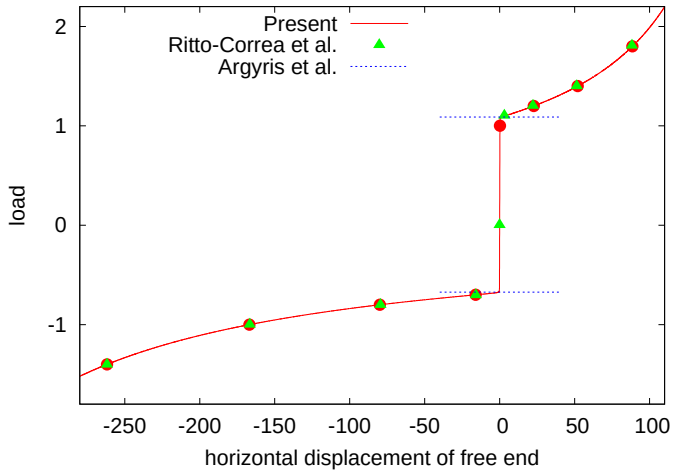

Figure 5: Lateral-torsional buckling of right-angle frame: load-displacement.

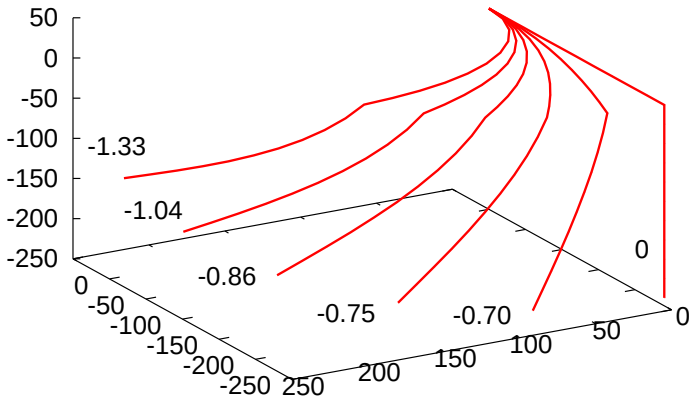

Figure 6: Lateral-torsional buckling of right-angle frame: deformed shapes; labels indicate the value of the load.

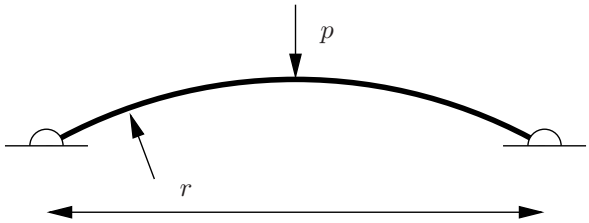

Figure 7: Pinned beam sketch.

Table 3: Pinned beam non-dimensional data.

Radius, r	1.0
Arc angle, ψ	$\pi/3$
Section width, b	0.1
Section height, h	0.02
Young's modulus	1.0×10^9
Poisson's ratio	0.3
Shear factor, κ	5/6

the beam. Figure 6 shows a three-dimensional view of the deformation of the structure for selected load levels. The results are in good agreement with those reported in [32].

4.4 Buckling of Pinned Beam

The arc-shaped beam of Fig. 7 is considered, with pinned ends. This numerical example is original; it has been developed purposely to assess the proposed formulation. The arc radius r is equal to 1. Since the arc spans 60 degrees ($\pi/3$), the distance between the hinges is equal to r. Data are summarized in Table 3. A transverse load is applied at the center of the beam.

As the load is increased, the solution evolves through several buckling conditions and turning points (which appear as points on the z-p curve whose tangent is vertical), as illustrated in Fig. 8. Figures 9 and 10 respectively show the deformed shapes at turning points and at null load conditions. This example is the generalization to a (discretized) deformable continuum of the bi-stable spring considered in Section 4.1. The proposed approach could easily pass through several turning points with no convergence issues using an increment $\Delta s = 0.1$ with a weight of 10^{-6} on the load and neglecting the rotation parameters in the normalization of the solution increment.

4.5 Pinched Cylindrical Shell Mounted Over Rigid Diaphragms

This problem, reported as test 3.6 in Sze et al. [39] (Fig. 11) and analyzed by several authors, has been used to validate the original four-node nonlinear shell element based on the Enhanced Assumed Strain (EAS) and Assumed Natural Strain (ANS) formulations and implemented in MBDyn [40, 41].

Table 4: Pinched cylindrical shell non-dimensional data.

Length, ℓ	200.0
Radius, R	100.0
Thickness, h	1.0
Young's modulus	3.0×10^4
Poisson's ratio	0.3
Maximum load, P	1.2×10^4

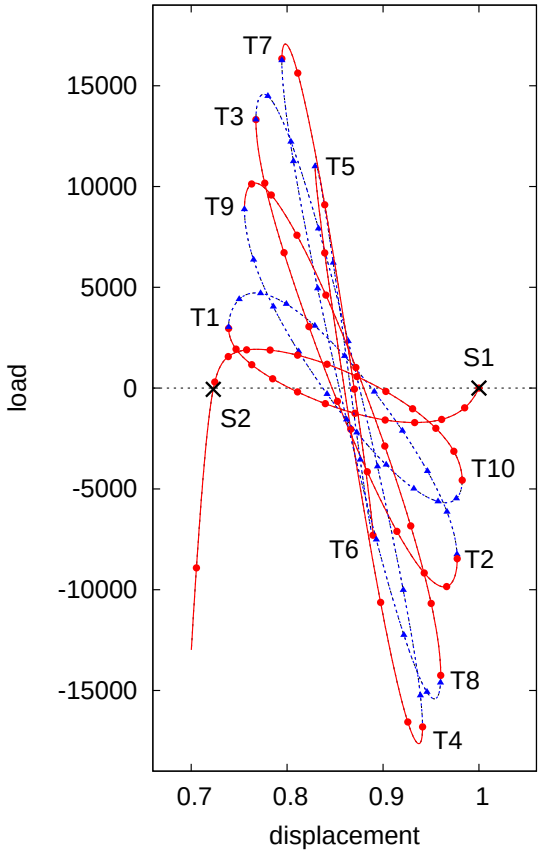

Figure 8: Buckling of pinned beam: load vs. transverse displacement; T1–10 are turning points; S1 and S2 are the initial and final stable null load solutions.

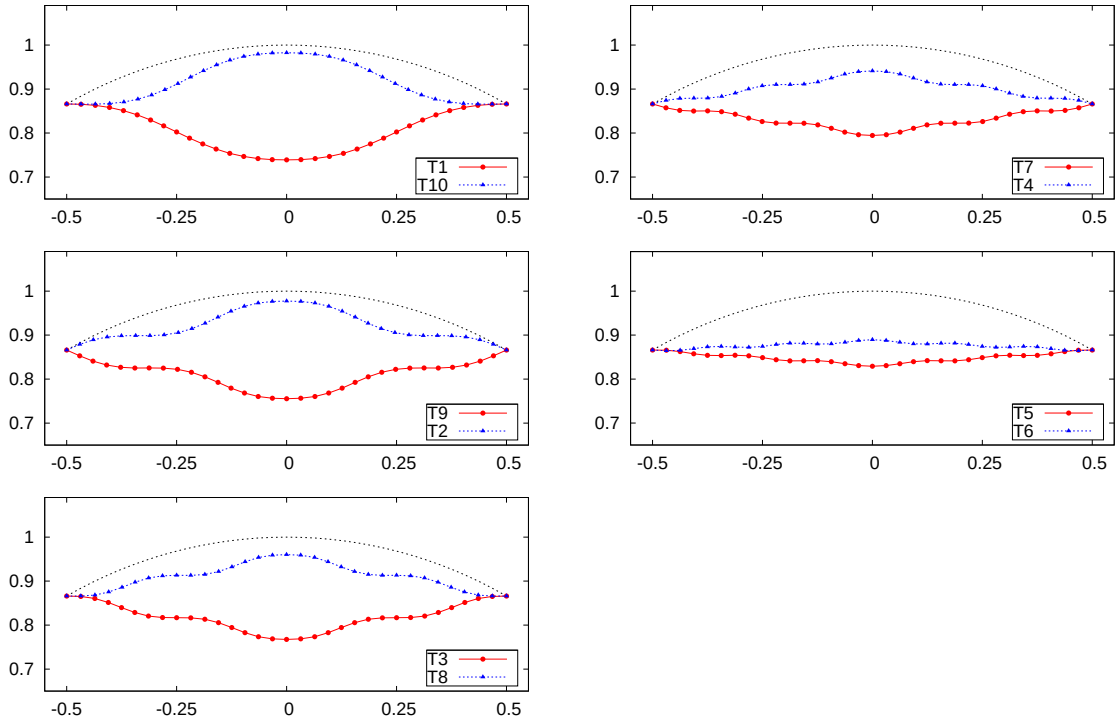

Figure 9: Buckling of pinned beam: deformed shapes at turning points.

A cylindrical shell is mounted on rigid end diaphragms which restrain the in-plane (radial and tangential) displacement components of the free ends of the cylinder, whereas the axial components are permitted. The properties are reported in Table 4. The system is loaded by opposite vertical compression forces p applied in point A and its symmetric counterpart, which are located on the top and bottom of the mid-span circumference.

A 48×48 mesh of four-node shell elements is used to model one eighth of the cylinder, with appropriate symmetry constraints as discussed in [39], resulting in 2401 structural nodes and a total of 31070 equations, including those related to kinematic constraints, the strain enhancement equations of the shell elements and the proposed load increment formulation.

The plots of Figs. 12 monitor the vertical radial displacement of point A, W_{A}, and the horizontal radial displacement of point B, U_{B}; the latter point is located on the horizontal symmetry plane of the problem. They compare the present results with those provided in [39], which were computed using Riks' algorithm in the finite element solver Abaqus.

Figure 12(a) shows that a prescribed displacement increment strategy (imposing the vertical displacement of point A, and interpreting the corresponding reaction force as the load p) was unable to go past the near-snapthrough that occurs when p is about 2000. The need to solve this problem, and the impossibility to go past the snapthrough condition at $p \approx 2000$ shown in Fig. 12(a) by prescribing the displacement, actually motivated the development of the incremental loading capability for MBDyn that is the subject of this work. When the proposed procedure is applied, the solution converges smoothly (Fig. 12(b)), requiring no more than 3 to 4 iterations per step. Little more than 200 load steps are required to exceed by more than four times the maximum load considered in [39] for this test case (Fig. 12(c)).

Figure 12(c) clearly shows how the load can be increased well beyond the ultimate load considered in [39]. In the final part of the analysis, for $p \approx 40000$, the load needs to significantly reduce for a

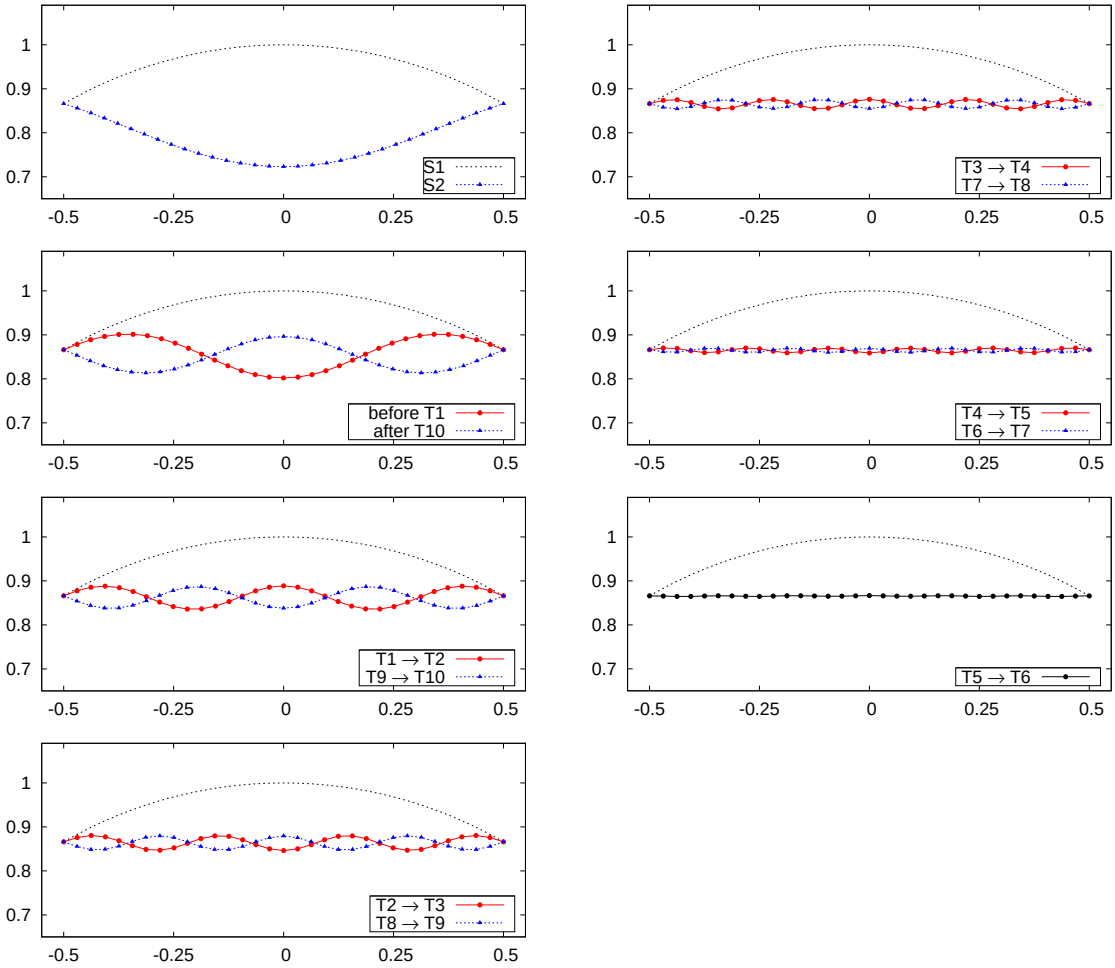

Figure 10: Buckling of pinned beam: deformed shapes at zero load configurations.

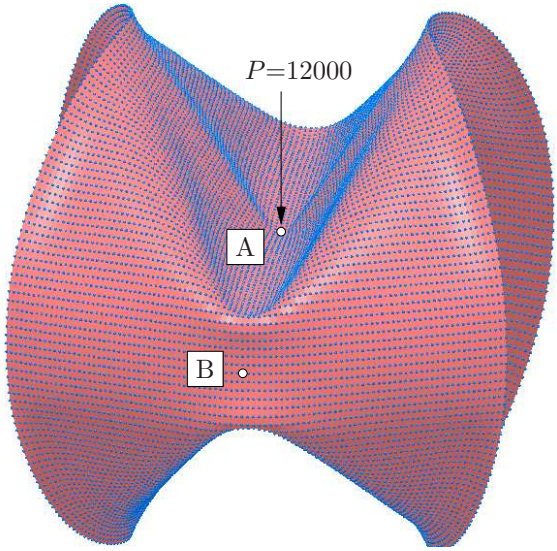

Figure 11: Pinched cylindrical shell mounted over rigid diaphragms.

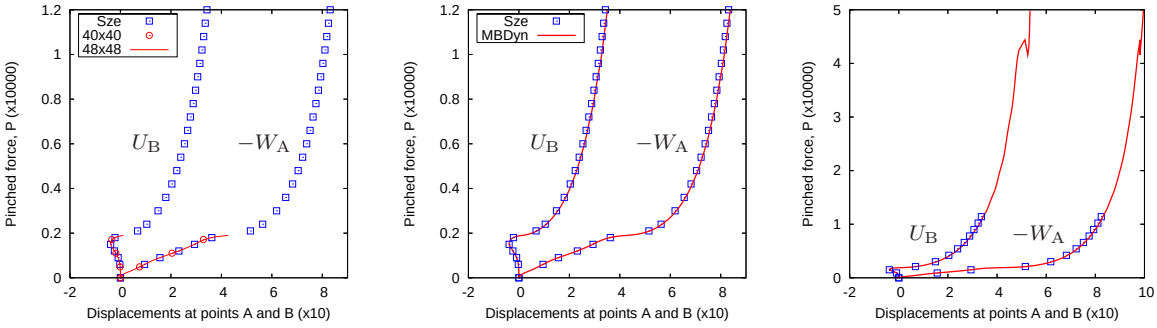

(a) Incremental displacement.

(b) Pseudo-arc lenght incr. load.

(c) Pseudo-arc lenght incr. load, $P_{\max} > 4{\times}P$, the max value in [39].

Figure 12: Pinched cylindrical shell mounted over rigid diaphragms.

Table 5: Static twisting of a slender bar: properties (from [42]).

Young's modulus, E	200.0	GPa
Poisson's modulus, ν	0.32	
Density ρ	7860.0	kg/m^3
Bar length, L	1.0	m
Section radius, r	0.5	mm
Axial stiffness, EA	1.5708×10^{5}	N
Shear stiffness, GA	5.9500×10^{4}	N
Torsional stiffness, GJ	7.4375×10^{-3}	N·m^2
Bending stiffness, EJ	9.8175×10^{-3}	N·m^2
Mass per unit span, m	6.1732×10^{-3}	kg/m
Gravity acceleration, g	9.81	m/s^2

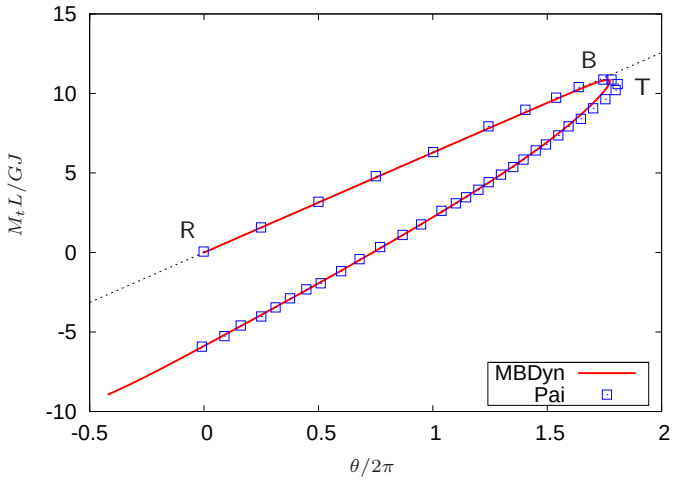

Figure 13: Static twisting of a slender bar: moment-rotation curve (Pai, [42]); 'R': reference point, 'B': bifurcation, 'T': turning point along the low energy branch of the secondary path.

while; nonetheless, no significant deterioration of the quality of the convergence is observed.

4.6 Static Twisting of a Slender Bar

The analysis proposed by Pai in Section 5.2 of [42] is presented here. An initially straight bar is clamped at one end and can slide along the undeformed axis at the other end. The section of the bar is circular; it is made of homogeneous isotropic material. The dimensions and the structural properties are reported in Table 5.

The end of the bar in (1,0,0) is clamped, whereas the one in (0,0,0) can slide along the x axis. The sliding end of the rod cannot rotate about axes y and z, whereas its rotation about axis x is prescribed using the proposed formulation.

The problem is modeled using 10 three-node finite volume beam elements [37], for a total of 21 nodes. The mid-point static deflection of the beam under gravity is about 16 mm, in accordance with [42].

The curve in Fig. 13 shows the normalized torsional moment, M_tL/GJ, applied to the sliding end of the bar, as a function of the rotation θ about the x axis. The present results correlate very well with the solution obtained in [42] up to the first bifurcation, followed by a turning point. In its

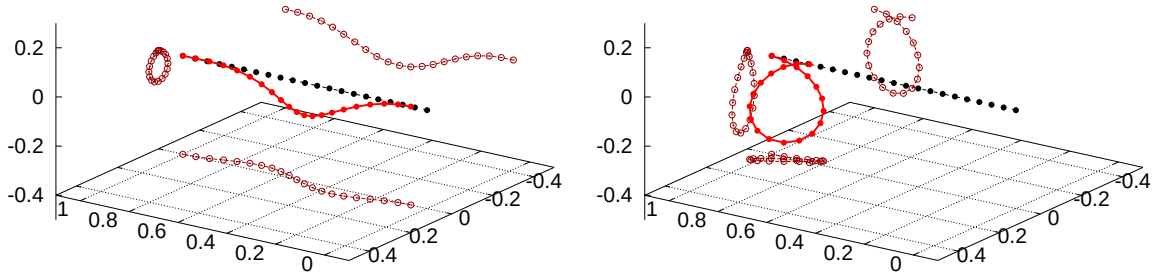

(a) $\theta \cong 2\pi$, $M_t L/GJ \cong 10$

(b) $\theta \cong 0\pi$, $M_t L/GJ \cong -6$

Figure 14: Static twisting of a slender bar: deformed shapes.

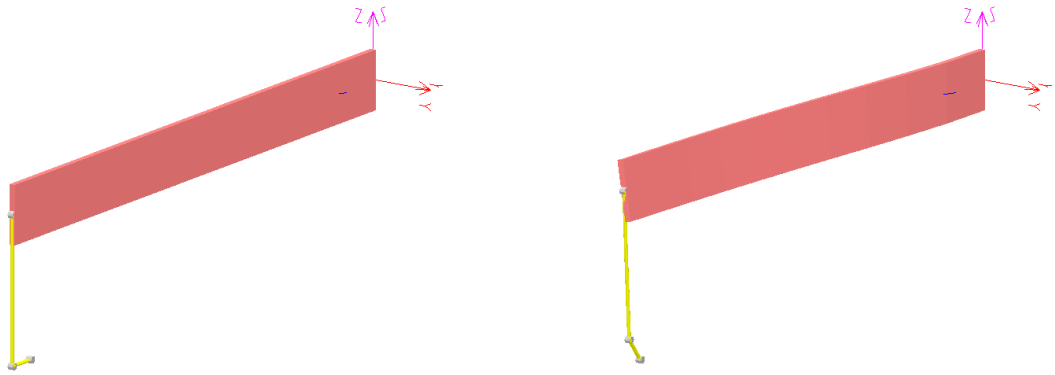

(a) Initial configuration.

(b) Buckled configuration.

Figure 15: Lateral buckling

present form, the proposed formulation is not able to follow the unstable branches of the curve. On the contrary, by simply prescribing the rotation of the sliding end of the bar the analysis completely misses the bifurcation and fails shortly after it, along the unstable branch, for $\theta \approx 3.8\pi$.

Two snapshots of the deformed shape are presented in Fig. 14: the one in Fig. 14(a) is in the vicinity of the turning point, while that of Fig. 14(b) is taken where the rotation approaches zero, well after the bifurcation, for a negative value of the torsional moment (according to Fig. 13).

4.7 Lateral Buckling

This problem has been proposed as a benchmark to test the effects of geometrical nonlinearity in a dynamic context. It is considered, for example, in [43] and [44] to compare several formulations and implementations of geometrically nonlinear beams within the framework of multibody dynamics.

In the original form, a cantilever beam is bent in its plane of greatest flexural rigidity, up to the point that triggers lateral buckling. In the context of dynamics, when buckling occurs the beam snaps laterally and twists, inducing highly oscillatory motion. In the present context of (quasi-)static non-linear analysis, when buckling occurs the problem becomes ill-conditioned.

As shown in Fig. 15, the beam is clamped at one end. The length is 1 m; the cross-section is rectangular, 100 mm high and 10 mm wide. To induce the snapping, a tip load is imposed at the free

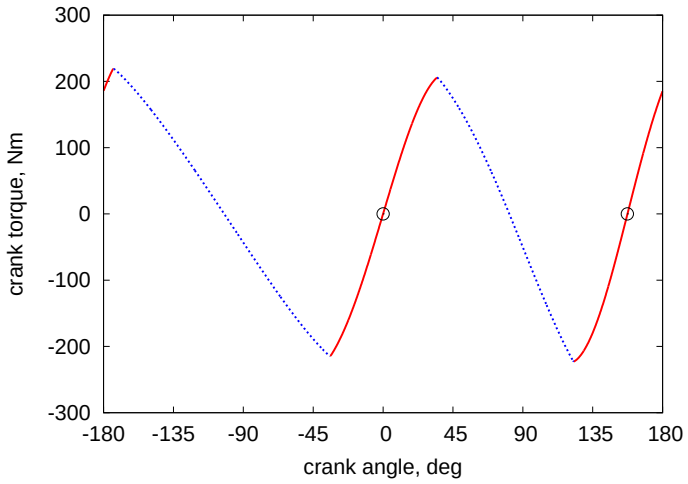

Figure 16: Lateral buckling: crank load vs. crank angle; circles indicate stable equilibrium points.

end by means of a rotating crank and a vertical rod. The rod is connected to the beam by a spherical joint and to the crank by a Cardano joint. An initial imperfection is simulated by laterally displacing the vertical bar and the crank by 0.1 mm. The length of the crank is 0.05 m, with circular section of 24 mm diameter, whereas the vertical rod length is 0.25 m, with circular section of 48 mm diameter. All parts are made of aluminum, with Young modulus $E = 73$ GPa and Poisson ratio $\nu = 0.3$. The beam is modeled using five three-node elements, whereas both the crank and the rod are modeled using a single three-node beam element each.

As discussed for example in [43], the dynamic solution provided by the proposed multibody implementation is in excellent agreement with state-of-art flexible multibody formulations. When performing a quasi-static analysis, the direct solution fails in the vicinity of buckling because of the ill-conditioning of the problem.

Figure 15(b) shows the buckled configuration obtained using the proposed formulation. The incrementally applied load is represented by the torque that acts on the crank about the axis of the revolute joint that connects it to the ground. Figure 16 shows the moment applied to the crank as a function of the crank angle. This example illustrates the application of the proposed approach to a problem with typical features of flexible mechanisms.

5 Conclusions

A method for the introduction of a pseudo-arc length analysis in general-purpose multibody dynamics formulations is proposed. The proposed development provides general-purpose software with the capability to analyze systems subjected to bifurcations and turning points, i.e. so-called buckling conditions. The proposed development is minimally intrusive: although access to the source code of the free general-purpose multibody software MBDyn was available, in this work the functionality has been formulated as a run-time loadable element, with no need to modify the original code. A comparable amount of intrusiveness is expected when considering closed-source software that support user-defined elements.

Funding

This research received no specific grant from any funding agency in the public, commercial, or not-for-profit sectors.

Acknowledgments

The contribution of Marco Morandini and Riccardo Vescovini to the implementation of the shell element is gratefully acknowledged.

References

[1] Walter E. Haisler, James A. Stricklin, and John E. Key. Displacement incrementation in non-linear structural analysis by the self-correcting method. *Intl. J. Num. Meth. Engng.*, 11(1):3–10, 1977. doi:10.1002/nme.1620110103.

[2] Jean-Louis Batoz and Gouri Dhatt. Incremental displacement algorithms for nonlinear problems. *Intl. J. Num. Meth. Engng.*, 14(8):1262–1267, 1979. doi:10.1002/nme.1620140811.

[3] E. Riks. An incremental approach to the solution of snapping and buckling problems. *Intl. J. Solids Structures*, 15(7):529–551, 1979. doi:10.1016/0020-7683(79)90081-7.

[4] M.A. Crisfield. A fast incremental/iterative solution procedure that handles "snap-through". *Computers & Structures*, 13(1–3):55–62, June 1981. doi:10.1016/0045-7949(81)90108-5.

[5] M. A. Crisfield. An arc-length method including line searches and accelerations. *Intl. J. Num. Meth. Engng.*, 19(9):1269–1289, September 1983. doi:10.1002/nme.1620190902.

[6] J. L. Meek and Hoon Swee Tan. Geometrically nonlinear analysis of space frames by an incremental iterative technique. *Comput. Meth. Appl. Mech. Engng.*, 47(3):261–282, December 1984. doi:10.1016/0045-7825(84)90079-3.

[7] K. H. Schweizerhof and P. Wriggers. Consistent linearization for path following methods in nonlinear FE analysis. *Comput. Meth. Appl. Mech. Engng.*, 59(3):261–279, December 1986. doi:10.1016/0045-7825(86)90001-0.

[8] Bruce W. R. Forde and Siegfried F. Stiemer. Improved arc length orthogonality methods for nonlinear finite element analysis. *Computers & Structures*, 27(5):625–630, 1987. doi:10.1016/0045-7949(87)90078-2.

[9] J. L. Meek and S. Loganathan. Geometrically non-linear behaviour of space frame structures. *Computers & Structures*, 31(1):35–45, 1989. doi:10.1016/0045-7949(89)90165-X.

[10] Reijo Kouhia and Martti Mikkola. Tracing the equilibrium path beyond simple critical points. *Intl. J. Num. Meth. Engng.*, 28(12):2923–2941, December 1989. doi:10.1002/nme.1620281214.

[11] Murray J. Clarke and Gregory J. Hancock. A study of incremental-iterative strategies for non-linear analyses. *Intl. J. Num. Meth. Engng.*, 29(7):1365–1391, May 1990. doi:10.1002/nme.1620290702.

[12] Z. Chen and H. L. Schreyer. Secant structural solution strategies under element constraint for incremental damage. *Comput. Meth. Appl. Mech. Engng.*, 90(1–3):869–884, September 1991. doi:10.1016/0045-7825(91)90188-C.

[13] Eugene L. Allgower and Kurt Georg. Continuation and path following. *Acta Numerica*, 2:1–64, 1993. doi:10.1017/S0962492900002336.

[14] E. Carrera. A study on arc-length-type methods and their operation failures illustrated by a simple model. *Computers & Structures*, 50(2):217–229, 1994. doi:10.1016/0045-7949(94)90297-6.

[15] Y. T. Feng, D. Perić, and D. R. J. Owen. Determination of travel directions in path-following methods. *Mathematical and Computer Modelling*, 21(7):43–59, April 1995. doi:10.1016/0895-7177(95)00030-6.

[16] Y. T. Feng, D. Perić, and D. R. J. Owen. A new criterion for determination of initial loading parameter in arc-length methods. *Computers & Structures*, 58(3):479–485, February 1996. doi:10.1016/0045-7949(95)00168-G.

[17] K. A. Lazopoulos. Second order displacement fields of a thick elastic plate under thrust — the incompressible case. *Intl. J. Solids Structures*, 33(3):433–449, January 1996. doi:10.1016/0020-7683(95)00039-D.

[18] K. A. Lazopoulos and S. Markatis. Compound branching in elastic systems. *Comput. Meth. Appl. Mech. Engng.*, 135(1–2):187–200, August 1996. doi:10.1016/0045-7825(95)00979-5.

[19] A. Cardona and A. Huespe. Nonlinear path following with turning and bifurcation points in multibody systems analysis. In *Computational methods in applied sciences '96*, Paris, France, September 9–13 1996.

[20] Alberto Cardona and Alfredo Huespe. Evaluation of simple bifurcation points and post-critical path in large finite rotation problems. *Computer Methods in Applied Mechanics and Engineering*, 175(1–2):137–156, 1999. doi:10.1016/S0045-7825(98)00365-X.

[21] H.-B. Hellweg and M. A. Crisfield. A new arc-length method for handling sharp snap-backs. *Computers & Structures*, 66(5):704–709, March 1998. doi:10.1016/S0045-7949(97)00077-1.

[22] E. A. de Souza Neto and Y. T. Feng. On the determination of the path direction for arc-length methods in the presence of bifurcations and 'snap-backs'. *Comput. Meth. Appl. Mech. Engng.*, 179(1–2):81–89, August 1999. doi:10.1016/S0045-7825(99)00042-0.

[23] F. Taheri and S. Moradi. A robust methodology for the simulation of postbuckling response of composite plates. *Computational Mechanics*, 26(3):295–301, 2000. doi:10.1007/s004660000173.

[24] K. K. Choong and J.-Y. Kim. A numerical strategy for computing the stability boundaries for multiloading systems by using generalized inverse and continuation method. *Engineering Structures*, 23(6):715–724, June 2001. doi:10.1016/S0141-0296(00)00071-7.

[25] Kurt Georg. Matrix-free numerical continuation and bifurcation. *Numerical Functional Analysis and Optimization*, 22(3 & 4):303–320, June 2001. doi:10.1081/NFA-100105106.

[26] Anders Eriksson and Costin Pacoste. Element formulation and numerical techniques for stability problems in shells. *Comput. Meth. Appl. Mech. Engng.*, 191(35):3775–3810, July 2002. doi:10.1016/S0045-7825(02)00288-8.

[27] Eduard Riks. Buckling. In Erwin Stein, René de Borst, and Thomas J. R. Hughes, editors, *Encyclopedia of Computational Mechanics*, volume 2: Solids and Structures, chapter 4. John Wiley & Sons, 2004. doi:10.1002/0470091355.ecm027.

[28] V. Mallardo and C. Alessandri. Arc-length procedures with BEM in physically nonlinear problems. *Engineering Analysis with Boundary Elements*, 28:547–559, 2004. doi:10.1016/j.enganabound.2003.11.002.

[29] Xiao-zu Su Bashir-Ahmed Memon. Arc-length technique for nonlinear finite element analysis. *Journal of Zhejiang University SCIENCE*, 5(5):618–628, 2004.

[30] Li Yuanqi and Shen Zuyan. Improvements on the arc-length-type method. *Acta Mechanica Sinica*, 20(5):541–550, October 2004. doi:10.1007/BF02484277.

[31] Michael Müller. Passing of instability points by applying a stabilized NewtonRaphson scheme to a finite element formulation: Comparison to arc-length method. *Computational Mechanics*, 40:683–705, 2007. doi:10.1007/s00466-006-0133-y.

[32] Manuel Ritto-Corrêa and Dinar Camotim. On the arc-length and other quadratic control methods: Established, less known and new implementation procedures. *Computers & Structures*, 86:1353–1368, 2008. doi:10.1016/j.compstruc.2007.08.003.

[33] Reijo Kouhia. Stabilized forms of orthogonal residual and constant incremental work control path following methods. *Comput. Meth. Appl. Mech. Engng.*, 197(13–16):1389–1396, February 2008. doi:10.1016/j.cma.2007.11.002.

[34] Pierangelo Masarati, Marco Morandini, and Paolo Mantegazza. An efficient formulation for general-purpose multibody/multiphysics analysis. *J. of Computational and Nonlinear Dynamics*, 9(4):041001, 2014. doi:10.1115/1.4025628.

[35] A. Fumagalli, P. Masarati, M. Morandini, and P. Mantegazza. Control constraint realization for multibody systems. *J. of Computational and Nonlinear Dynamics*, 6(1):011002 (8 pages), January 2011. doi:10.1115/1.4002087.

[36] J. C. Simo and L. Vu-Quoc. A three-dimensional finite strain rod model. part II: Computational aspects. *Comput. Meth. Appl. Mech. Engng.*, 58:79–116, 1986. doi:10.1016/0045-7825(86)90079-4.

[37] Gian Luca Ghiringhelli, Pierangelo Masarati, and Paolo Mantegazza. A multi-body implementation of finite volume beams. *AIAA Journal*, 38(1):131–138, January 2000. doi:10.2514/2.933.

[38] Pierangelo Masarati. Adding kinematic constraints to purely differential dynamics. *Computational Mechanics*, 47(2):187–203, 2011. doi:10.1007/s00466-010-0539-4.

[39] K. Y. Sze, X. H. Liu, and S. H. Lo. Popular benchmark problems for geometric nonlinear analysis of shells. *Finite Elements in Analysis and Design*, 40:1551–1569, 2004. doi:10.1016/j.finel.2003.11.001.

[40] Pierangelo Masarati, Marco Morandini, Giuseppe Quaranta, and Riccardo Vescovini. Multibody analysis of a micro-aerial vehicle flapping wing. In J. C. Samin and P. Fisette, editors, *Multibody Dynamics 2011*, Brussels, Belgium, July 4–7 2011.

[41] Marco Morandini and Pierangelo Masarati. Implementation and validation of a 4-node shell finite element. In *ASME IDETC/CIE 2014*, Buffalo, NY, August 17–20 2014. DETC2014-34473.

[42] P. Frank Pai. Three kinematic representations for modeling of highly flexible beams and their applications. *Intl. J. Solids Structures*, 48(19):2764–2777, 2011. doi:10.1016/j.ijsolstr.2011.06.001.

[43] O. A. Bauchau, G. Wu, P. Betsch, A. Cardona, J. Gerstmayr, B. Jonker, P. Masarati, and V. Sonneville. Validation of flexible multibody dynamics beam formulations using benchmark problems. In *3rd Joint International Conference on Multibody System Dynamics - IMSD 2014*, Busan, Korea, June 30-July 3 2014.

[44] Alessandro Tasora and Pierangelo Masarati. Analysis of rotating systems using general-purpose multibody dynamics. In *IFToMM ICORD 2014*, Milan, Italy, September 22–25 2014.